Research Article Vol. 31, No. 4 / 13 Feb 2023 / Optics Express 5801
Optics EXPRESS

# Quantitative study of birefringence effects in fiber-based orthogonal-pump FWM systems

HAO LIU,* KYLE R. H. BOTTRILL, VALERIO VITALI, AUSTIN TARANTA, AND PERIKLIS PETROPOULOS

*Optoelectronics Research Centre, University of Southampton, Southampton SO17 1BJ, UK*
*hl1a18@soton.ac.uk*

**Abstract:** Optical fibers have unwanted residual birefringence due to imperfections in fabrication processes and environmental conditions. This birefringence will randomize the state of polarization of propagating signals and may harm the performance of four-wave mixing based processing devices. Here, we present a quantitative study of the effects of birefringence in orthogonal-pump four-wave mixing systems, and identify different regions of operation of the optical fiber, mainly determined by the relative magnitude between the physical length $L$ and beat length $L_b$. This finding clarifies the characteristics of the complex interplay between birefringence and four-wave mixing and advises appropriate fiber length selection for minimized polarization dependent gain.



## 1. Introduction

Four-wave mixing (FWM) processes based on Kerr nonlinearity in optical fibers have been shown to enable a number of all-optical signal processing devices in the past two decades, such as wavelength converters [1,2], optical phase conjugators [3–5] and phase-sensitive amplifiers [6,7]. These all-optical systems could become an important part of future high-capacity wavelength division multiplexing (WDM) networks, thanks to their potential for operating over an ultra-wide bandwidth and with low latency.

There are a variety of nonlinear media commonly used for FWM, including silicon [8–10] silicon nitride [11–15] and semiconductor optical amplifiers (SOAs) [16–19], which are promising for all-optical signal processing applications. Notably, silicon and SOAs have demonstrated their potential in performing polarization-insensitive signal processing operations [20–22], when engineered appropriately. All the same, owing to its low coupling losses (when spliced) and low propagation loss, optical fiber (in particular, highly nonlinear fiber (HNLF) [23,24] with low dispersion), remains a popular medium in which to perform FWM.

For many FWM processes, a non-birefringent fiber is desirable. However, in practice, real-world fiber samples will generally possess some small residual birefringence, leading to them being described as "lowly birefringent" fibers. Such fibers [23] are known to exhibit a stochastic, longitudinal variation in core diameter, which in turn leads to a longitudinally varying birefringence. The longitudinally varying birefringence randomizes the polarization state of input signals and makes FWM-based devices more polarization sensitive, which can be particularly detrimental to applications where polarization-insensitivity is desired [25]. It is well-known that the distribution of fiber birefringence differs from sample to sample, even in those taken from the same fiber spool, making the exact behavior of a given system less predictable, compounding commercialisation of fiber-based FWM techniques.

#480274 https://doi.org/10.1364/OE.480274
Journal © 2023 Received 8 Nov 2022; revised 13 Jan 2023; accepted 16 Jan 2023; published 2 Feb 2023

Optics EXPRESS

Although some experimental demonstrations attempt to resolve polarisation sensitivity problems by relying on external compensation techniques [1,2,26], such approaches are time-consuming and difficult to optimise experimentally. Aside from advances in fabrication or control of extrinsic causes of birefringence (such as spool diameter, fiber bending, etc.), there is little that can be done to avoid the effects of birefringence upon a FWM system other than controlling the fiber length. Although in literature it is well known that low polarization sensitivity can be achieved in short lowly birefrigent fiber or long highly birefringent fiber [27], there has been no direct study to date on the dependency of polarization sensitivity in FWM systems upon the total length of a given sample of fiber. In this work, we study this exact dependency, quantifying the effects of birefringence in terms of conversion efficiency (CE) and polarisation dependent gain (PDG) of a non-degenerate FWM system in a fiber with longitudinally varying fiber birefringence, parameterised by two statistical metrics: fiber length to beat length ratio ($L/L_b$) and fiber length to correlation length ratio ($L/L_c$). Numerical studies are presented in this work, in which multiple instances of birefringent fiber were generated using the random modulus model (RMM) [28] and the resulting idler PDGs of an orthogonally polarized FWM system, found using a coupled Nonlinear Schrödinger Equation (C-NLSE) [29,30], were compared using a Monte-Carlo methodology. We have found that different regions of operation in the optical fibers, determined by the $L/L_b$ ratio, reveal different inherent contributions to the polarization sensitivity in an orthogonally-pumped FWM system, resulting from the complex interplay between the randomly varying birefringence and FWM. In addition, contrary to what might be expected, we show that an isotropic fiber (with low $L/L_b$ and $L/L_c$) is not the only solution exhibiting low PDG, and that, perhaps more importantly, there exists a range of $L/L_b$ and $L/L_c$ values that should be avoided when targeting low PDG in orthogonally pumped FWM systems.

## 2. Method

This numerical study utilizes a C-NLSE to simulate continuous-wave (CW) propagation in optical fiber, incorporating both linear and nonlinear birefringence effects. $E_x$ and $E_y$ are the transverse components of complex electric fields. By considering $E_x$ and $E_y$ as the slowly-varying envelopes of the electric field components, the C-NLSE in the time domain takes the form:

$$\frac{\partial E_x}{\partial z} - i\frac{\Delta\beta_{xy}}{2}E_x - \frac{\Delta\beta'_{xy}}{2}\frac{\partial E_x}{\partial t} = i\gamma[(P_x + \frac{2}{3}P_y)E_x + \frac{1}{3}(E_y)^2E_x^*] \tag{1}$$

$$\frac{\partial E_y}{\partial z} + i\frac{\Delta\beta_{xy}}{2}E_y + \frac{\Delta\beta'_{xy}}{2}\frac{\partial E_y}{\partial t} = i\gamma[(P_y + \frac{2}{3}P_x)E_y + \frac{1}{3}(E_x)^2E_y^*] \tag{2}$$

where $P_x = E_xE_x^*$ and $P_y = E_yE_y^*$, $\gamma$ is the nonlinearity coefficient, $\Delta\beta_{xy}/2 = (\beta_x(\omega_c) - \beta_y(\omega_c))/2$ represents the birefringence strength (half of the difference between the propagation constants along horizontal '$x$' and vertical '$y$' directions) at the center frequency $\omega_c$. $\Delta\beta'_{xy}/2$ represents the first order derivative of birefringence strength with respect to the angular frequency at $\omega_c$. Here and further in the paper, $\Delta\beta'_{xy}$ is approximated as $\Delta\beta_{xy}/\omega_c$ [28,31], which holds good for the bandwidths we are studying [32,33]. $\Delta\beta'_{xy}$ accounts for the differential polarization variations among signals with different frequencies and is responsible for the polarization mode dispersion (PMD) [25]. The three nonlinear birefringence terms on the right-hand side of equation (1) and (2) respectively act as the self-phase modulation (SPM) [29,34], cross-phase modulation (XPM) [29,34] and ellipse rotation [29,34] terms, which are relevant to the following investigation.

The fiber was divided into $N$ short segments in order to emulate weakly birefringent fibers whose birefringence varies continuously. $\Delta\beta_{xy}$ and $\Delta\beta'_{xy}$ differed in each fiber segment and were assigned in accordance with the used birefringence model. The rotation angle of the birefringent axis was introduced at the beginning of each fiber segment. $\Delta\beta_{xy}$, $\Delta\beta'_{xy}$ and birefringent axis rotation angle were modelled using the RMM as this model has been shown to be in agreement

Optics EXPRESS

with experimental results [35]. RMM assumes that the first two components of the birefringence vector $\frac{\overrightarrow{\Delta\beta_{xy}}}{2}$ independently obey the Langevin equation [28] and allows fibers to be modelled with a birefringence that varies randomly along their length, determined by two parameters: fiber beat length $L_b$ and fiber correlation length $L_c$. $L_b$ represents a length scale over which a signal restores its original state of polarization (SoP). The stronger the local birefringence, the shorter the distance a signal will take to recover its original SoP. $L_c$ represents how fast the random perturbation in a fiber occurs [36], which is governed by $\left\langle \frac{\overrightarrow{\Delta\beta_{xy}(0)}}{2} \cdot \frac{\overrightarrow{\Delta\beta_{xy}(z)}}{2} \right\rangle = \frac{\Delta\beta_{xy}^2(0)}{2} \exp(-z/L_c)$[28]. $L_c$ varies from fiber sample to fiber sample and also depends upon how a given sample is spooled (tension, spool diameter, etc.). By assigning the values of $L_b$ and $L_c$, we were able to generate the longitudinal profiles of fibers with varying birefringence strength and birefringent axis rotation angles (as shown for two example realizations in Figs. 1(c),(d)). The length of each fiber segment $dz$ was chosen to be much smaller than either of $L_b$ or $L_c$ to avoid artificially overestimating the effects of fiber birefringence upon parametric devices using a short fiber length [29]. Since RMM directly simulates $\Delta\beta_{xy}(\omega, z)$ without using $\Delta n(\omega, z)$ (the difference between the refractive indices along horizontal "$x$" and vertical "$y$" directions), this helps to isolate the effect of dispersion variations from fiber birefringence [29]. The C-NLSE was numerically integrated by using the split-step Fourier method (SSFM) [34], where birefringence and nonlinear terms were solved respectively in the frequency and the time domain sequentially for each fiber segment.

The FWM system studied in this work was the orthogonally pumped, non-degenerate system, which is known to offer polarization insensitive wavelength conversion of signals in isotropic fiber [2,3]. As shown in Fig. 1(a), the initial spectrum (input to the C-NLSE) consisted of two horizontally and vertically polarized pumps (along the $x$ and $y$ axes, respectively) and a signal, whose SoP can be varied. Here and in the rest of the paper, the spacing between the two pumps was assumed to be 974 GHz (correspond to 8 nm at 1570 nm). This pump spacing was essentially inspired by an experimental set-up we have been studying [38], wherein a pump spacing of 8 nm was used, resulting in relatively low exposure to dispersion. In addition, we maintained this spacing for easier future comparison with experimental results. We only consider this one fixed pump spacing as it was found that different pump spacings did not change the main findings of this work (please see Fig. S1–Fig. S6 in Supplement 1). The linear birefringence rotates a signal's SoP around the axis of the first component of the Stokes vector ($S_1$), leaving $S_1$ unchanged. The nonlinear effects induced nonlinear polarization rotation (NPR) will render a signal's SoP rotating around the axis of the third component of the Stokes vector ($S_3$), leaving $S_3$ unchanged. Thus, for a CW signal propagating along a fiber which is several beat lengths long, the interplay between linear birefringence and NPR can produce quite a complex polarization evolution on the Poincaré sphere [34,39]. It needs to be noted that a signal's SoP will experience NPR only if its ellipticity is non-zero. [34,39]. For a randomly birefringent fiber, the birefringent axis rotation, combined with birefringence strength, will randomly scatter the signal's SoP on the Poincaré sphere so that the signal's zero ellipticity cannot be maintained along the fiber. To illustrate this point, we compared two 200-m long fibers in Figs. 2(a),(b): 1) an isotropic fiber, and 2) a weakly, randomly birefringent fiber (one fiber realization with $L/L_b = 0.01$ and $L/L_c = 1$) under the condition of 2 rad nonlinear phase shift (NPS), $\phi = \gamma\sqrt{P_1 P_2}L$, where $\gamma$ is the fiber nonlinear coefficient, $P_1$ and $P_2$ are the two input pump power levels and $L$ is the fiber length. Two pumps' SoPs are launched horizontally (along '$x$' axis) and vertically polarized (along '$y$' axis). We can see that the pump can maintain its zero ellipticity only in the isotropic fiber, while in the weakly birefringent fiber, its SoP randomly scattered around the $S_3$ axis because NPR takes place once the pump's SoP gains some ellipticity. This happens even in implementations with very weak birefringence. In addition, since $S_3$ is involved in the NPR, a change in the sign of $S_3$ resulting from linear birefringence would cause the sign of the nonlinear phase shift to also alternate, so that the effect of NPR upon a signal tends to be averaged out [39]. Thus, the two

Optics EXPRESS

orthogonally polarized pumps may start to experience NPR at the beginning of the fiber even in a weakly and randomly birefringent fiber, and the two pumps may lose their original orthogonality relation unless a proper fiber birefringence is chosen.

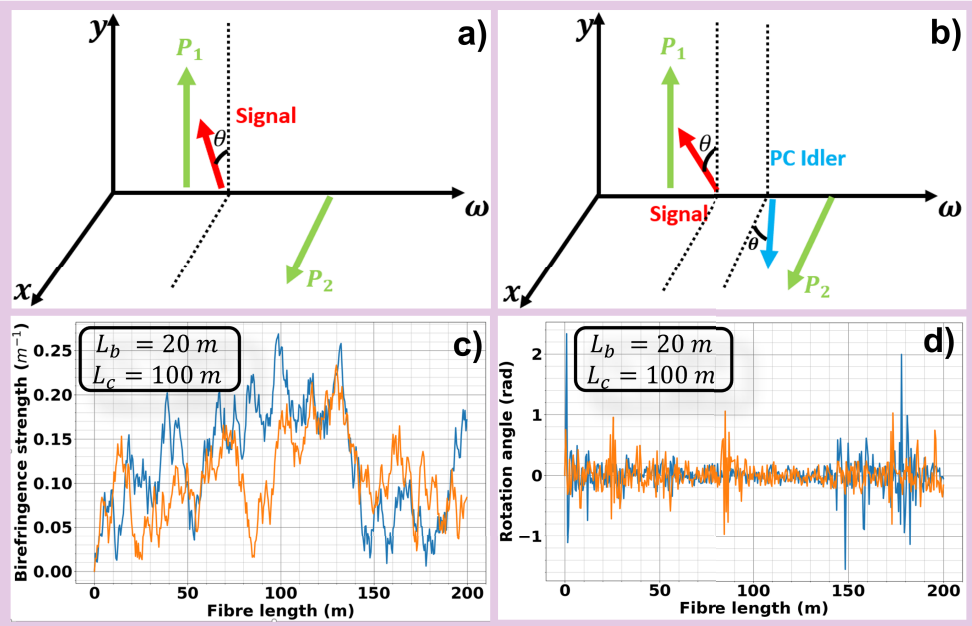


**Fig. 1.** FWM spectrum for the input (a) and output (b) of HNLF; (c) birefringence strength profiles for two different realizations ($L_b$ = 20m, $L_c$ = 100m); (d) angle rotation of birefringence axis for two different realizations ($L_b$ = 20m, $L_c$ = 100m) [37].

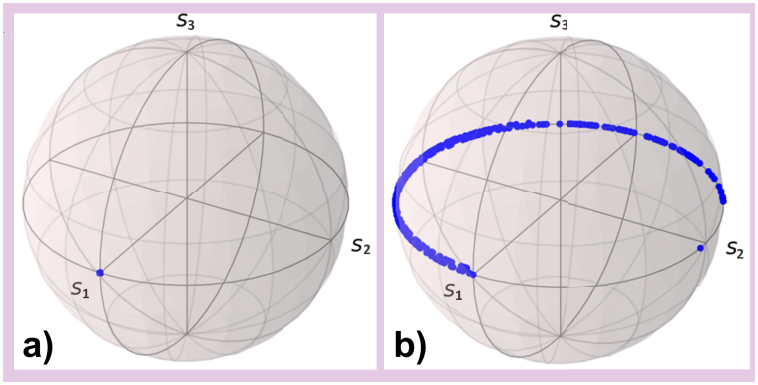


**Fig. 2.** Poincaré sphere representation of the polarization evolution for a pump in an orthogonally-pump FWM system in a 200 m long fiber (a) without and (b) with random birefringence (one fiber realization with $L/L_b$ = 0.01 and $L/L_c$ = 1) for 2 rad NPS [37].

In this system, the SoP of the input signal was initially obtained by sweeping the phase difference and the orientation angle of two orthogonal electric field components from 0 to $2\pi$ and 0 to $\pi/2$, respectively. By selecting different step sizes of the phase difference and the orientation angle, we performed a convergence test of the PDG for a signal with a frequency around 242 GHz away from $\omega_c$.We only consider this one fixed signal spacing as it was found that different

Optics EXPRESS

signal spacings did not change the main findings of this work (please see Fig. S7–Fig. S14 in Supplement 1). The convergence tests showed that at least 64 points were needed to achieve $< 0.2$ dB numerical error. For each input signal SoP, the idler power at the output of the fiber (see Fig. 1(b)) was recorded and compared to the input signal power to evaluate the conversion efficiency (CE). From these values, the PDG was obtained by finding the difference between maximum CE and minimum CE. The $<CE>_{pol}$ was obtained by averaging over the different CE values that resulted from each of the 64 different input signal SoP. The fiber was assumed lossless and dispersionless so that the effects of birefringence, specifically, could be isolated from any other effects. In keeping with this objective, the NPS was held constant, regardless of fiber length $L$, the two pump power levels $P_1$, $P_2$ and $\gamma$, so that any variations in CE could be attributed to birefringence only.

For a fixed $N$, $\phi$, $L/L_b$ and $L/L_c$, CE and PDG remain the same regardless of the fiber length chosen. Therefore, in our model, we considered the normalised length ratios $L/L_b$ and $L/L_c$. We swept the ratio $L/L_b$ between $10^{-2}$ and $10^2$, whilst $L/L_c$ was swept between $10^{-1}$ and $10^2$. With telecommunication fibers typically possessing an $L_b$ and $L_c$ of 5-50 m and 10-100 m respectively [40], this corresponds to fiber lengths within the broad range of roughly 5 cm to 10 km, inclusive of fiber lengths typically used in FWM experiments. We carried out a Monte-Carlo analysis, where 100 different realizations of the fiber were generated. This was verified to be a sufficient number for the obtained $<PDG>_{real}$ and $<<CE>_{pol}>_{real}$ values to show their dependency upon length ratios $L/L_b$ and $L/L_c$. $<..>_{real}$ and $<..>_{pol}$ represent a variable inside of the brackets that has been averaged over 100 different realizations and 64 different SoP, respectively. Additionally, in the following, $\sigma_{<CE>_{pol}}$ and $\sigma_{PDG}$ denote the standard deviation of $<CE>_{pol}$ and $PDG$ respectively, obtained from 100 different realizations.

## 3. Results and discussion

### 3.1. $<CE>_{pol}$ and PDG dependence upon $L/L_b$ and $L/L_c$

Figures 3(a),(c) and (b),(d) show the dependence of $<>CE>_{pol}>_{real}$ and $<PDG>_{real}$ respectively, on the length ratios $L/L_b$ and $L/L_c$ for two values of NPS, namely 0.3 rad and 2 rad, where the two input pump power levels were set to be the same. A NPS of 0.3 rad was assumed to result in little stimulated Brillouin scattering (SBS) in a typical nonlinear fiber [41], whilst a value of 2 rad would normally require some method of SBS suppression to be adopted, such as pump phase dithering [2,42]. Considering the two sets of graphs together, we can identify three banded regions, which are mainly determined by the length ratio $L/L_b$. The value of $<<CE>_{pol}>_{real}$ increases from band A to band C as we increase $L/L_b$ while keeping the same launching condition for the two pumps (as shown in Fig. 1(a)). Moreover, $<PDG>_{real}$ spikes in band B, an effect that is associated with the input pumps' NPS, whilst it decreases in band C, where the 'averaging' effect of NPR provided by random birefringence becomes dominant.

In band A, where the fiber length is much smaller than $L_b$, the fiber has extremely weak birefringence strength for the typical HNLF lengths used in FWM experiments. For example, $\Delta n$ in this band is on the order of $10^{-11}$ or $10^{-10}$ for a 200 m long fiber; such low values of birefringence may not be possible in practice. Nevertheless, as discussed both in the previous section and in the literature [34,39,43], even a small amount of birefringence may give rise to some NPR of the pump waves. This is evidenced in Fig. 4, where an orthogonal-pump FWM system with $L/L_b$ in the range $10^{-2}$ to $10^{-1}$ is shown to exhibit a relative increase in the PDG when the NPS values are varied from 0.3 rad to 4 rad. The $<PDG>_{real}$ performance deteriorates when the physical length is comparable to $L_b$ (band B). Compared to a fiber in Band A with the same physical length and assuming that the SoP of the two orthogonal pumps is linear at launch, it will take a shorter distance for the SoP of the two pumps to become elliptical, and the ellipticity of the two pumps will tend to be larger. Therefore, the NPR will take place earlier in the fiber and will be more pronounced, leading to a larger PDG at the fiber end (see Figs. 3(b),(d) and

Optics EXPRESS

Fig. 4). The shaded area in Fig. 4 represents $\sigma_{PDG}$. Both this parameter and $\sigma_{<CE>_{pol}}$ are shown in Fig. 5 for the whole parameter space for two values of NPS. This shows that when operating in Band B, both CE and PDG become susceptible to the exact fiber birefringence profile. Thus, it will be difficult for a fiber located in this region to achieve high CE and low PDG simultaneously, and the fiber behavior will differ from sample to sample.

When $L$ is more than ten times longer than $L_b$ (band C), $<PDG>_{real}$ decreases irrespective of the NPS used (shown in Figs. 3(b),(d)). As discussed in the previous section, the effect of NPR upon a signal will be averaged out because of the alternating signs of $S_3$ along propagation resulting from the linear birefringence. Therefore, a carefully chosen amount of birefringence can help reduce or eliminate the effects of NPR upon PDG. This characteristic is shown in Fig. 4, where the PDG evolution with $L/L_b$ is drawn for two different values of $L/L_c$. It is additionally observed that a large $L/L_c$ ratio can help prevent a further increase in PDG when $L/L_b$>10. Short $L_c$ tends to produce large birefringent axis rotation angle along a fiber. This, as a result, leads to the uniformly spread of the normalized signals' ellipticities ($S_3$) from -1 to 1, providing another degree of 'averaging' to the effects of NPR upon PDG. Additionally, as discussed in the previous section, frequency dependent birefringence introduces differential polarization variations among signals with different frequencies through PMD [25,44]. A short $L_c$ can help reduce the PMD so that the effects of PMD upon PDG can be decreased.

### 3.2. PDG and degree of co-polarization evolution

To gain further insights on the onset of PDG in a dual-orthogonal pump FWM system, we considered the examples of four different fiber samples selected from the three bands identified previously. All samples were chosen to have the same physical length of 200 m but they varied in their beat length. For simplicity, their $L/L_c$ ratios were kept constant and of a modest value (equal to 1.08). For each of these fiber samples, we considered three values of NPS (0.3, 2 and 4 rad) and studied the spatial evolution of both the PDG and pump SoP along the length of each sample.

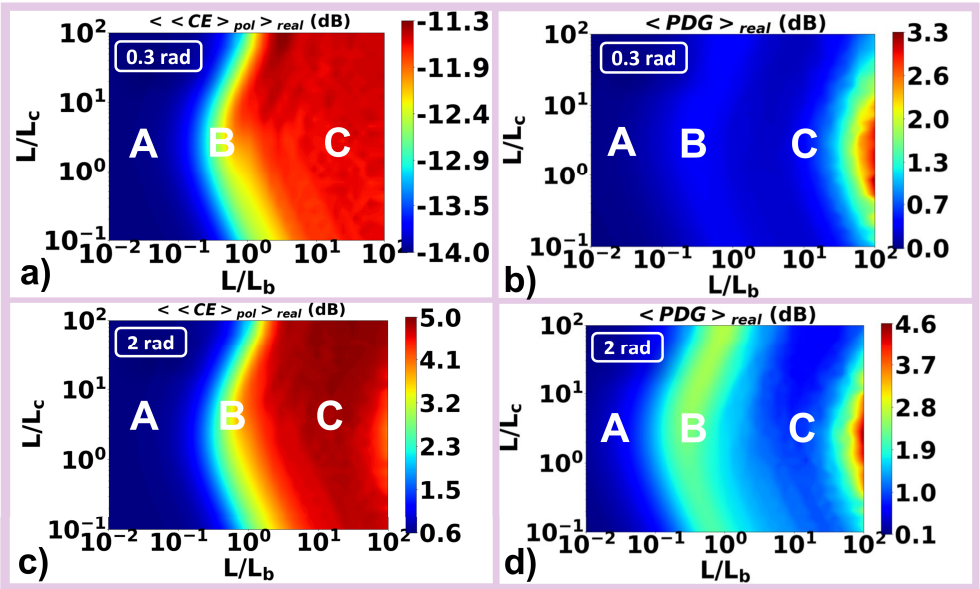


**Fig. 3.** (a) $<<CE>_{pol}>_{real}$ and (b) $<PDG>_{real}$ as a function of both length ratios $L/L_b$ and $L/L_c$ for 0.3 rad NPS value; (c) $<<CE>_{pol}>_{real}$ and (d) $<PDG>_{real}$ as a function of both length ratios $L/L_b$ and $L/L_c$ for 2 rad NPS value [37].

Optics EXPRESS

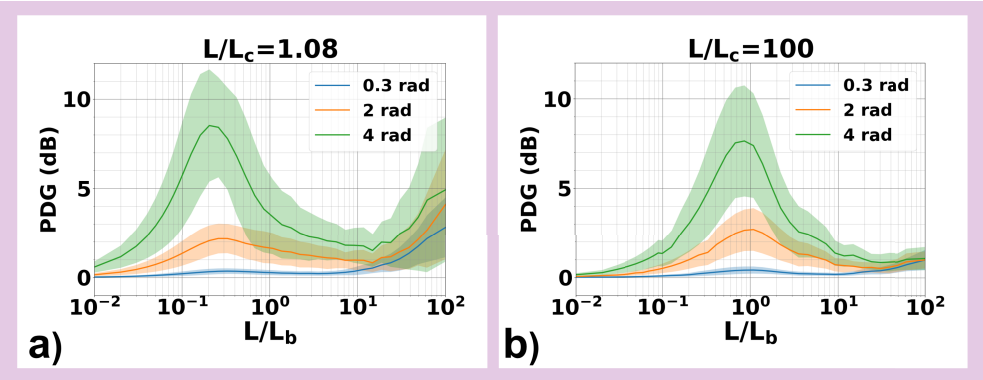


**Fig. 4.** PDG as a function of $L/L_b$ in the case of (a) $L/L_c = 1.08$; (b) $L/L_c = 100$ [37].

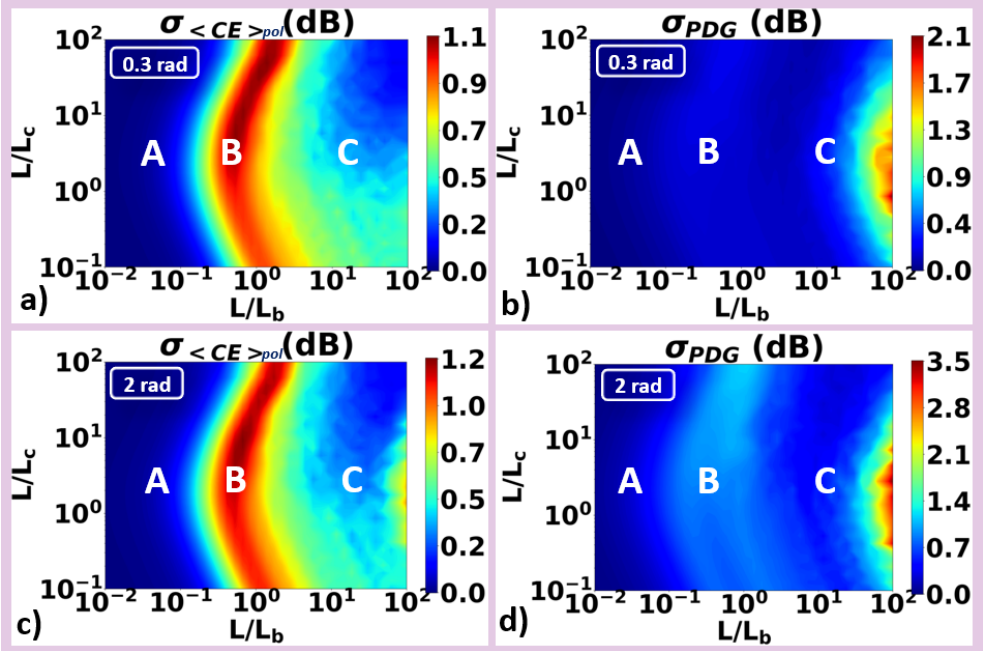


**Fig. 5.** (a) $\sigma_{<CE>_{pol}}$ and (b) $\sigma_{PDG}$ as a function of both length ratios $L/L_b$ and $L/L_c$ for 0.3 rad NPS value; (c) $\sigma_{<CE>_{pol}}$ and (d) $\sigma_{PDG}$ as a function of both length ratios $L/L_b$ and $L/L_c$ for 2 rad NPS value [37].

The degree of co-polarization between two pumps was defined as the dot product of the normalized Stokes parameters of the two pumps ($\vec{S_1} \cdot \vec{S_2}$), where the dot product values of -1 and 1 represent perfectly orthogonal (anti-parallel on the Poincaré sphere) and perfectly co-polarized SoPs, respectively [43]. Figures 6(a),(b) represent the cases of weakly birefringent fibers (fibers belonging in Bands A and B), where in line with the discussion presented above, the PDG evolution is closely associated with the degree of co-polarization evolution of the two pumps.

This, in turn, depends on both the pump power and the birefringence strength of the fiber. In contrast, when decreasing the beat length further (Fig. 6(c)), the PDG evolution is weakly dependent on the input NPS values. As discussed in the previous section, the alternating sign of

Optics EXPRESS

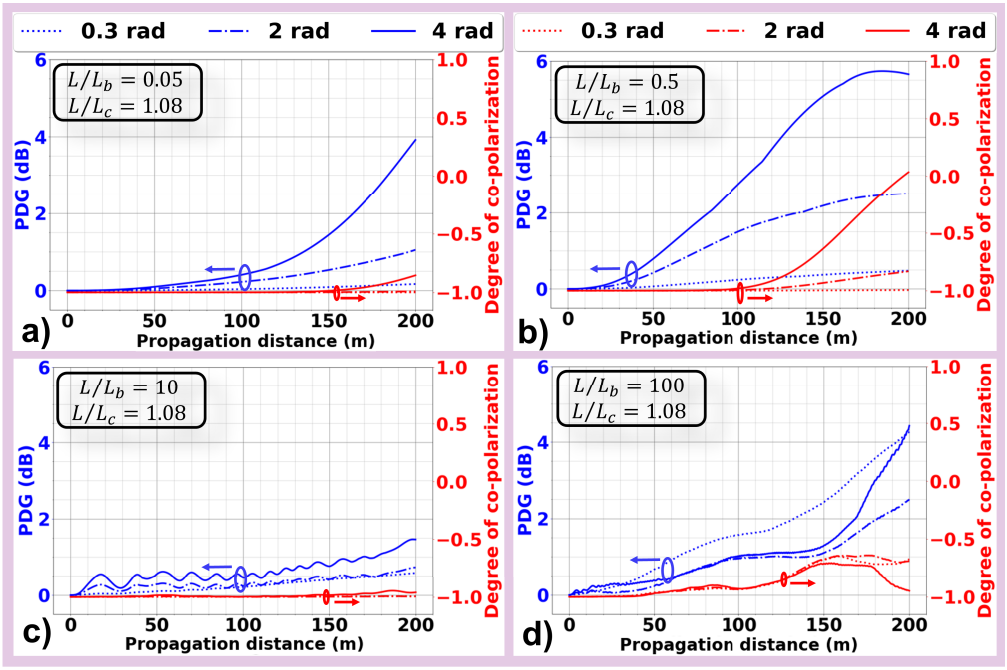


**Fig. 6.** The evolution of PDG and pumps degree of co-polarization for four different fiber samples with (a) $L/L_b = 0.05$, $L/L_c = 1.08$; (b) $L/L_b = 0.5$, $L/L_c = 1.08$; (c) $L/L_b = 10$, $L/L_c = 1.08$; (d) $L/L_b = 100$, $L/L_c = 1.08$ [37].

the ellipticity of the waves averages out the NPR and the pumps maintain their orthogonality to a great extent along the fiber length. The PDG evolution is observed to exhibit small ripples, which we attribute to the randomly varying birefringence of the fiber. The PDG evolution becomes less regular when the fiber birefringence is further increased (Fig. 6(d)). In this case, the frequency dependence of the birefringence is strong, leading the SoP of two pumps at different frequencies to rotate at different rates as they propagate along the fiber. In this scenario, the orthogonality relation between the two pumps exhibits a very weak dependence on the NPS (Fig. 6(d)).

## 4. Conclusion

We presented a quantitative study of the birefringence effects in fiber-based dual orthogonal-pump FWM systems. By utilizing the C-NLSE and RMM, we identified the relations between the fiber length, beat length and correlation length that minimize the polarization-dependent gain of the process. We identified three different bands, defined by these relations, and revealed the interplay between fiber birefringence and FWM that determined their respective behavior. The physical length of fibers in band A is one or two orders of magnitude shorter than their beat length, and are, therefore, nearly isotropic. In typical HNLFs, this corresponds to a length of only a few meters of fiber. To obtain a desirable CE performance, large pump powers or a fiber with a large nonlinear coefficient should be used, both of which could lead to technical challenges. Fibers in band B, where the fiber length is comparable to the beat length, may correspond to fiber lengths of tens of meters for a typical HNLF. The PDG is pump power dependent and dominated by NPR. Fibers in band C, where the fiber length is in the order of ten times longer than the beat length, may correspond to a physical length from several hundreds of meters to 1 km of fiber. Fibers in this band can exhibit low PDG and desirable CE simultaneously. In this band, the

Optics EXPRESS

magnitude of $L_c$ is found to be important in maintaining a low PDG. However, $L_c$ depends on external environmental conditions and may vary significantly in different spool diameters.

Therefore, factors like fiber spooling may need to be considered to ensure predictable operation. In the early 2000s, kilometer lengths of fiber were commonly used in FWM demonstrations [45], which would generally expect to lie in band C. Since then, there has been a trend of decreasing fiber length. Today, demonstrations using lengths as short as tens of meters [46] have been made and we might expect this fibers to typically lie in band B. As a result, a further shortening of the fiber might be expected (if PDG in the orthogonal pumped systems is a concern) or otherwise a engineering fiber further for reduced birefingence might be motivated. The presented results may provide new insights into exploiting and controlling the complex FWM dynamics in fiber systems and will ultimately help advise future FWM system designs.

**Funding.** Engineering and Physical Sciences Research Council (EP/S002871/1).

**Acknowledgments.** This work was supported by the UK's EPSRC through the project PHOS (EP/S002871/1). The authors acknowledge the use of the IRIDIS High Performance Computing Facility, and associated support services at the University of Southampton, in the completion of this work.

**Disclosures.** The authors declare no conflicts of interest.

**Data availability.** Data underlying the results presented in this paper are available in Ref. [37].

**Supplemental document.** See Supplement 1 for supporting content.

## References

1. S. Watanabe, T. Kato, T. Tanimura, C. Schmidt-Langhorst, R. Elschner, I. Sackey, C. Schubert, and T. Hoshida, "Wavelength conversion using fiber cross-phase modulation driven by two pump waves," Opt. Express **27**(12), 16767–16780 (2019).
2. V. J. Rancano, F. Parmigiani, P. Petropoulos, and D. J. Richardson, "100GHz grid-aligned reconfigurable polarization insensitive black-box wavelength converter," in *Optical Fiber Communication Conference* (Optical Society of America, 2013), paper JTh2A–19.
3. S. Yoshima, Y. Sun, Z. Liu, K. R. Bottrill, F. Parmigiani, D. J. Richardson, and P. Petropoulos, "Mitigation of nonlinear effects on WDM QAM signals enabled by optical phase conjugation with efficient bandwidth utilization," J. Lightwave Technol. **35**(4), 971–978 (2017).
4. Y. Sun, A. Lorences-Riesgo, F. Parmigiani, K. R. Bottrill, S. Yoshima, G. D. Hesketh, M. Karlsson, P. A. Andrekson, D. J. Richardson, and P. Petropoulos, "Optical nonlinearity mitigation of 6× 10 GBd polarization-division multiplexing 16 QAM signals in a field-installed transmission link," in *Optical Fiber Communication Conference* (Optical Society of America, 2017), paper Th3J–2.
5. X. Liu, A. Chraplyvy, P. Winzer, R. Tkach, and S. Chandrasekhar, "Phase-conjugated twin waves for communication beyond the kerr nonlinearity limit," Nat. Photonics **7**(7), 560–568 (2013).
6. P. A. Andrekson and M. Karlsson, "Fiber-based phase-sensitive optical amplifiers and their applications," Adv. Opt. Photonics **12**(2), 367–428 (2020).
7. Z. Tong, C. Lundström, P. Andrekson, C. McKinstrie, M. Karlsson, D. Blessing, E. Tipsuwannakul, B. Puttnam, H. Toda, and L. Grüner-Nielsen, "Towards ultrasensitive optical links enabled by low-noise phase-sensitive amplifiers," Nat. Photonics **5**(7), 430–436 (2011).
8. M. Pu, H. Hu, C. Peucheret, H. Ji, M. Galili, L. K. Oxenløwe, P. Jeppesen, J. M. Hvam, and K. Yvind, "Polarization insensitive wavelength conversion in a dispersion-engineered silicon waveguide," Opt. Express **20**(15), 16374–16380 (2012).
9. A. Gajda, L. Zimmermann, M. Jazayerifar, G. Winzer, H. Tian, R. Elschner, T. Richter, C. Schubert, B. Tillack, and K. Petermann, "Highly efficient cw parametric conversion at 1550 nm in soi waveguides by reverse biased pin junction," Opt. Express **20**(12), 13100–13107 (2012).
10. A. Gajda, L. Zimmermann, J. Bruns, B. Tillack, and K. Petermann, "Design rules for pin diode carriers sweeping in nano-rib waveguides on soi," Opt. Express **19**(10), 9915–9922 (2011).
11. Z. Ye, P. Zhao, K. Twayana, M. Karlsson, P. A. Andrekson, and V. Torres-Company, "Ultralow-loss meter-long dispersion-engineered silicon nitride waveguides," in *Conference on Lasers and Electro-Optics* (IEEE, 2021), pp. 1–2.
12. Z. Ye, P. Zhao, M. Karlsson, and P. A. Andrekson, "Ultralow-loss silicon nitride waveguides for parametric amplification," in *Optical Fiber Communication Conference* (Optica Publishing Group, 2022), paper W4J–3.
13. J. Liu, G. Huang, R. N. Wang, J. He, A. S. Raja, T. Liu, N. J. Engelsen, and T. J. Kippenberg, "High-yield, wafer-scale fabrication of ultralow-loss, dispersion-engineered silicon nitride photonic circuits," Nat. Commun. **12**(1), 1–9 (2021).

Optics EXPRESS


14. F. Gardes, A. Shooa, G. De Paoli, I. Skandalos, S. Ilie, T. Rutirawut, W. Talataisong, J. Faneca, V. Vitali, Y. Hou, T. D. Bucio, I. Zeimpekis, C. Lacava, and P. Petropoulos, "A review of capabilities and scope for hybrid integration offered by silicon-nitride-based photonic integrated circuits," Sensors **22**(11), 4227 (2022).
15. C. Lacava, S. Stankovic, A. Z. Khokhar, T. D. Bucio, F. Gardes, G. T. Reed, D. J. Richardson, and P. Petropoulos, "Si-rich silicon nitride for nonlinear signal processing applications," Sci. Rep. **7**(1), 22 (2017).
16. P. P. Baveja, D. N. Maywar, and G. P. Agrawal, "Interband four-wave mixing in semiconductor optical amplifiers with ase-enhanced gain recovery," IEEE J. Sel. Top. Quantum Electron. **18**(2), 899–908 (2012).
17. A. P. Anthur, R. Zhou, S. O'Duill, A. J. Walsh, E. Martin, D. Venkitesh, and L. P. Barry, "Polarization insensitive all-optical wavelength conversion of polarization multiplexed signals using co-polarized pumps," Opt. Express **24**(11), 11749–11761 (2016).
18. A. Sobhanan and D. Venkitesh, "Polarization-insensitive phase conjugation using single pump bragg-scattering four-wave mixing in semiconductor optical amplifiers," Opt. Express **26**(18), 22761–22772 (2018).
19. A. Sobhanan, A. Anthur, S. O'Duill, M. Pelusi, S. Namiki, L. Barry, D. Venkitesh, and G. P. Agrawal, "Semiconductor optical amplifiers: recent advances and applications," Adv. Opt. Photonics **14**(3), 571–651 (2022).
20. F. Da Ros, A. Gajda, E. P. da Silva, A. Peczek, A. Mai, K. Petermann, L. Zimmermann, L. K. Oxenløwe, and M. Galili, "Optical phase conjugation in a silicon waveguide with lateral pin diode for nonlinearity compensation," J. Lightwave Technol. **37**(2), 323–329 (2019).
21. A. Sobhanan, L. N. Venkatasubramani, R. D. Koilpillai, and D. Venkitesh, "Polarization-insensitive phase conjugation of qpsk signal using bragg-scattering fwm in soa," IEEE Photonics Technol. Lett. **31**(12), 919–922 (2019).
22. C. Lacava, M. A. Ettabib, and P. Petropoulos, "Nonlinear silicon photonic signal processing devices for future optical networks," Appl. Sci. **7**(1), 103 (2017).
23. Y. Yamamoto, Y. Tamura, and T. Hasegawa, "Silica-based highly nonlinear fibers and their applications," SEI Tech. Rev. **83**, 15–20 (2016).
24. H. Liu, K. R. Bottrill, V. Vitali, A. Taranta, and P. Petropoulos, "Birefringence effects in fibre-based polarisation-insensitive FWM systems," in *Conference on Lasers and Electro-Optics* (IEEE, 2022), pp. 1–2.
25. Q. Lin and G. P. Agrawal, "Effects of polarization-mode dispersion on fiber-based parametric amplification and wavelength conversion," Opt. Lett. **29**(10), 1114–1116 (2004).
26. M. Stephens, V. Gordienko, and N. Doran, "20 dB net-gain polarization-insensitive fiber optical parametric amplifier with> 2 THz bandwidth," Opt. Express **25**(9), 10597–10609 (2017).
27. S. Radic and C. McKinstrie, "Two-pump fiber parametric amplifiers," Opt. Fiber Technol. **9**(1), 7–23 (2003).
28. W. Huang and D. Yevick, "Polarization mode dispersion in short fiber lengths," J. Opt. Soc. Am. A **23**(6), 1509–1512 (2006).
29. M. Marhic, A. Rieznik, G. Kalogerakis, C. Braimiotis, H. Fragnito, and L. Kazovsky, "Accurate numerical simulation of short fiber optical parametric amplifiers," Opt. Express **16**(6), 3610–3622 (2008).
30. M. E. Marhic, *Fiber Optical Parametric Amplifiers, Oscillators and Related Devices* (Cambridge University Press, 2008).
31. C. Menyuk, "Application of multiple-length-scale methods to the study of optical fiber transmission," J. Eng. Math. **36**(1/2), 113–136 (1999).
32. W. Eickhoff, Y. Yen, and R. Ulrich, "Wavelength dependence of birefringence in single-mode fiber," Appl. Opt. **20**(19), 3428–3435 (1981).
33. Y. Ohtsuka, "Optical-frequency dependent modal birefringence and polarization mode dispersion of birefringent single-mode optical fibers over a broadband optical wavelength range," Opt. Rev. **8**(6), 498–499 (2001).
34. G. P. Agrawal, "Nonlinear fiber optics," in *Nonlinear Science at the Dawn of the 21st Century* (Springer, 2000), pp. 195–211.
35. A. Galtarossa, L. Palmieri, M. Schiano, and T. Tambosso, "Statistical characterization of fiber random birefringence," Opt. Lett. **25**(18), 1322–1324 (2000).
36. M. Guasoni, F. Parmigiani, P. Horak, J. Fatome, and D. J. Richardson, "Intermodal four-wave mixing and parametric amplification in kilometer-long multimode fibers," J. Lightwave Technol. **35**(24), 5296–5305 (2017).
37. H. Liu, K. R. H. Bottrill, V. Vitali, A. Taranta, and P. Petropoulos, "Quantitative study of birefringence effects in fibre-based orthogonal-pump fwm systems," (2022), last accessed 23 January 2023, https://doi.org/10.5258/SOTON/D2349.
38. K. R. Bottrill, N. Taengnoi, H. Liu, R. Kakarla, Y. Hong, and P. Petropoulos, "Suppression of spurious mixing in fwm-based systems through mid-span pump phase shift," in *Optical Fiber Communications Conference and Exhibition* (IEEE, 2022), pp. 1–3.
39. H. Ibarra-Villalon, O. Pottiez, A. Gómez-Vieyra, J. Lauterio-Cruz, and Y. Bracamontes-Rodriguez, "Numerical study of polarization evolution governed by linear birefringence, twist-induced circular birefringence and nonlinear birefringence in a single-mode optical fiber," J. Opt. **23**(12), 123501 (2021).
40. C. R. Menyuk and B. S. Marks, "Interaction of polarization mode dispersion and nonlinearity in optical fiber transmission systems," J. Lightwave Technol. **24**(7), 2806–2826 (2006).
41. V. Gordienko, Á. Szabó, M. Stephens, V. Vassiliev, C. Gaur, and N. Doran, "Limits of broadband fiber optic parametric devices due to Stimulated Brillouin Scattering," Opt. Fiber Technol. **66**, 102646 (2021).
42. K. Wong, M. Marhic, and L. Kazovsky, "Phase-conjugate pump dithering for high-quality idler generation in a fiber optical parametric amplifier," IEEE Photonics Technol. Lett. **15**(1), 33–35 (2003).

Optics EXPRESS

43. Q. Lin and G. P. Agrawal, "Vector theory of four-wave mixing: polarization effects in fiber-optic parametric amplifiers," J. Opt. Soc. Am. B **21**(6), 1216–1224 (2004).
44. F. Yaman, Q. Lin, and G. P. Agrawal, "Effects of polarization-mode dispersion in dual-pump fiber-optic parametric amplifiers," IEEE Photonics Technol. Lett. **16**(2), 431–433 (2004).
45. T. Tanemura and K. Kikuchi, "Polarization-independent broad-band wavelength conversion using two-pump fiber optical parametric amplification without idler spectral broadening," IEEE Photonics Technol. Lett. **15**(11), 1573–1575 (2003).
46. K. R. Bottrill, F. Parmigiani, D. J. Richardson, and P. Petropoulos, "Field trial of a scheme to overcome channel contention using all-optical wavelength conversion," in *European Conference on Optical Communication* (IEEE, 2017), pp. 1–3.